Research Square

Preprints are preliminary reports that have not undergone peer review.
They should not be considered conclusive, used to inform clinical practice,
or referenced by the media as validated information.

Synthesis, characterization, and application of nanohybrid formed by mixing carboxylated cellulose nanocrystal and zinc nitrate hexahydrate by precipitation method using Oxytenanthera abyssinica as raw material

Limenew Abate Worku
Addis Ababa Science and Technology University
Rakesh Kumar Bachheti (rkbachheti@gmail.com)
Addis Ababa Science and Technology University
Mesfin Getachew Tadesse
Addis Ababa Science and Technology University
Archana Bachheti
Graphic Era University

Research Article

Keywords: CNC/ZnO nanohybrids, Carboxylated cellulose nanocrystal, Antibacterial activities, Photocatalytic activities, Oxytenanthera abyssinica

Posted Date: November 4th, 2022

DOI: https://doi.org/10.21203/rs.3.rs-2225634/v1

License: This work is licensed under a Creative Commons Attribution 4.0 International License. Read Full License

Abstract

In this study, cellulose from Oxytenanthera abyssinica was hydrolyzed to create carboxylated cellulose nanocrystals in a solution of citric acid and sulfuric acid. Afterward, nanohybrids were synthesized using carboxylated cellulose nanocrystals, zinc nitrate hexahydrate for photocatalytic degradation, and antibacterial and antioxidant properties. The experimental results were characterized using FTIR, XRD, SEM, and UV-Vis spectroscopy. Data from SEM, XRD, DLS, and FTIR spectra showed that ZnO nanoparticles were loaded on carboxylated CNC to form a nanohybrid of CNC/ZnO with mean nanoparticles size of 164.18 nm and size distribution between 94–351 nm. The data showed CNC/ ZnO nanohybrid had higher antibacterial, photocatalytic and antioxidant activities than CNC. The higher antibacterial activity was observed against both grams positive (Klebsiella pneumonia and Escherichia coli) and gram-negative bacteria (Staphylococcus epidermidis and Staphylococcus aureus) with an inhibition zone of 26.00±1.00 to 41.33±1.15 mm in comparison with Ciprofloxacin. The maximal amount of methylene blue photodegradation (about 91.52%) was seen after 75 minutes of exposure to a UV lamp. 53.151.03% DPPH radical scavenging actives with IC50 value of 117.66 µm/ml were obtained at 125 µm/ml concentration of CNC/ZnO sample. Biomedical and environmental applications of cellulose are limited by its extremely low antibacterial, photocatalytic, and antioxidant properties. Therefore, this study was done to enhance these properties by synthesizing a nanohybrid of cellulose nanocrystals from cellulose produced from Oxytenanthera abyssinica and ZnO inorganic salt.

1. Introduction

Cellulose is the most important material found in nature, which has been applied in various applications due to its low toxicity, biocompatibility, and biodegradability (Kwok et al. 2017). It can be found in various substances, including tunicate, algae, fungi, natural fibers, wood, and bamboo (Wang et al. 2021). Cellulose is the primary raw material for the preparation of cellulose nanocrystals (CNC)(Reid et al. 2017).

For the past 20 years, academic research has focused on CNC due to its biodegradability, superior biocompatibility, high crystallinity, and excellent characteristics, such as large surface area, outstanding mechanical strength, and ease of chemical modification (Håkansson et al. 2014; Thomas et al. 2018). Due to these remarkable characteristics, CNC has much potential in the fields of devices that store energy (Chen et al. 2018; Kim et al. 2019), rheology modifiers (Hubbe et al. 2017; Liu et al. 2017), reinforcing agents (Clarkson et al. 2021; Zheng and Pilla, 2020), in the treatment of wastewater (Abouzeid et al. 2018; Dong et al. 2021), biomedical components (Du et al. 2019; Lin et al. 2019), and electrically flexible materials (Miao et al. 2020; Zhao et al. 2021). However, its applicability is constrained by its poor UV permeability, poor moisture stability, and lack of antioxidant and antibacterial properties. As a result, limitations to the use of CNC in the fields of biomedicine and photocatalysis. The hydroxyl functional groups on the CNC surface, however, serve as reactive platforms that allow chemical modification for the addition of new functional groups to improve the material's antibacterial, antioxidant and photocatalytic capabilities (Tao et al. 2020).

Metallic nanoparticles having favorable chemical and physical behavior are essential nanoscale materials successfully exploited in polymer functionalization (Azizi et al. 2014). Inorganic nanoparticles, ZnO nanoparticles are relatively non-toxic, affordable, and have exceptional optical performance properties such as photocatalytic, electrical, antibacterial, and other capabilities (Kołodziejczak-Radzimska and Jesionowski 2014). The utilization of ZnO in wastewater treatment has also recently received attention because of its capacity to degrade contaminants, such as organic dyes in water and heavy metals, removable during the purification of contaminated water (Samadi et al. 2016; Sharma et al. 2019; Guan et al. 2019). Unfortunately, the ZnO NPs small size and high surface free energy quickly clump together. To overcome this drawback, scientists are highly interested in synthesizing ZnO nanoparticles based on another substance, functioning as a carrier to improve the dispersion of ZnO nanoparticles at the nanoscale level (Tomczak et al. 2009). In this regard, combining CNC as template with ZnO nanoparticles has gained popularity, and studies have been conducted to modify

and functionalize cellulose nanocrystals to prevent ZnO nanoparticle aggregation(Tomczak et al. 2009; Yang et al. 2016; Yu et al. 2015).

There have been few publications on the formation of ZnO nanoparticles on cellulose substrates, even though research on cellulose-based nanocomposite materials is still ongoing. Most of the reported studies require complex synthesis procedures and time-consuming methods to prepare CNC. Since they mostly use inorganic acids (sulfuric acid, nitric acid, hydrochloric acid, etc) to hydrolysis cellulose, there are weak electrostatic interactions between Zn^{2+} and OH-groups on CNC. Thus, in this study, CNC/ZnO nanohybrids were synthesized using carboxylated CNC and $N_2O_6Zn.6H_2O$ as starting materials for antibacterial, antioxidant, and photodegradation applications. We use Organic acid (citric acid) to hydrolyze cellulose derived from lowland Ethiopian bamboo (*Oxytenathera abyssinica)* as a nanocrystalline cellulose source abundantly in the western part of Ethiopia.

2. Experimental

2.1 Materials and equipment

We employed analytical-grade chemicals in our investigation. In this investigation, the main chemicals used were CNC obtained from *Oxytenantheraabyssinica,* Zinc nitrate ($N_2O_6Zn.6H_2O$) (99%,FARIDABAD-121005, INDIA), sulfuric acid (98%, India), citric acid anhydrous (CHEMICALS UDYLOG-121001 (India), and sodium hydroxide (ALPHA CHEMIKA, India), sodium chloride (Maharashtra, India). All chemicals were acquired from the Charcos market center found in Addis Abeba, Ethiopia (Rankem India). The following instruments and equipment were frequently employed in these studies: sonicator (Intelligent Ultrasonic Processor), freeze dryer, *centrifuges (*Microfuge Centurion Scientific PrO-Analytical C1015), Zeta sizer (Malvern Zeta Nano (ZE3600), Oven, Analytical balance for laboratories (Ceramic-technology weight sensor), dialysis tube, digital hot plate, Stirrer, XRD (SHIMADZU XRD-6000), SEM, TGA 55-TA Instruments and *iS50 FTIRS* spectrometer, UV-Vis spectrophotometer Perkin Elmer UV–Vis spectroscope (USA).

2.2 The study area

Oxytenanthera abyssinica plant species were gathered from Pawe woreda, found in the Metekel zone, the western part of Ethiopia, as shown in Fig. 1. The area is situated between 36°20' and 36°32' longitude and 11°12' and 11°21' latitude. It is found at 1120 meters above sea level. The woreda has a hot, humid climate with temperatures ranging between 19.4 to 37.6°C, and receives 1586.32 mm of rain annually (Miruts, 2020). Of the total land of Pawe woreda, 30.6% is forest; among these, *Oxytenanthera abyssinica* is a botanical plant found in forests (Ambawu, 2019). A permition was obtained from the Pawe Woreda office of Agricultural and Rural Development to collect plant material based on support from Addis Abeba Science and Technology University.

2.3 Sample collection

Oxytenanthera, abyssinica plants with an average age of three years, were randomly collected from the study area by TAPPI standards from 2002 (TAPPI, 2002). The plant material was gathered and delivered to Addis Abeba University for botanical identification. The identification was carried out by taxonomist Doctor Endale Adam and Mr. Wogayew using the Flora of Eritrea and Ethiopia's taxonomic keys, as well as by comparison with the real specimens. This study has followed international, national, and institutional regulations in using plant components (IUCN, 1989).

2.4 Preparation of cellulose nanocrystal

Oxytenanthera abyssinica (COA) cellulose hydrolyzed by citric acid anhydrous (CAA) using Sulfuric acid (SA) as catalyst to produce the carboxylated CNC samples based on the methods used by Xu et al. (2017). Two grams of COA and (100

mL solution of 90 wt% CAA and 10% SA) was added to form solution. The solution was stirred with the Mixstab TEFAL Swing. The reactions were carried out in a spherical flask using an oil bath at 80 °C for 5 hours with a magnetic stirrer operating at 1000 rpm. After the hydrolysis reactions, hot distilled water (100 mL) was added to halt the process and avoid CAA crystallization. The subsequent step involved centrifuging the mixture for 15 minutes at 1000 rpm. The residue obtained after each centrifugation was rinsed with DI water three times. A dialysis tube was then used to dialyze the sediments until the solution's pH and conductivity were constant with distilled water. Using a probe ultrasonicator, the suspension was sonicated for 15 minutes at 25 kHz after diluting to a consistency of around 1wt% to create a uniformly dispersed aqueous solution known as CNC.

2.5 Preparation of ZnO/CNC nanohybrids

CNC has a remarkable ability to absorb metallic cations since it has several hydroxyl groups in its structure. Electrostatic interactions between Zn^{2+} and the oxygen atoms of hydroxyls allowed Zn^{2+} to be absorbed during the initial phase of the process. After NaOH was added, $Zn(OH)_2$ was gradually produced. ZnO was produced under thermal conditions, as indicated by scheme1 and Fig. 2 (Azizi et al. 2014).

In this research work, nanohybrids of CNC/ZnO were synthesized using a modified version of the technique utilized by Yu et al. (2015). Different weights of 0.1 mol/L aqueous solutions of $Zn(NO_3)_2$. $6H_2O$ was mixed with the carboxylated CNC produced in the above procedure in weight ratios of 0.25, 0.50, 0.75, and 1.00. These four samples were adjusted to a pH of 7 using 0.5 mol/L solutions of NaOH. To thoroughly precipitate Zn^{2+}, the mixture was then vigorously agitated while being heated to 80 ^oC and adding 0.1 M NaOH solutions were drop by drop. The carboxylates (COO-) of CNCs and Zn^{2+} were electrostatically attracted to one another, and $Zn(OH)_2$ precipitated. At 12,000 rpm, the mixture was centrifuged in DI water, at 10 ^oC, for 20 minutes to eliminate any byproducts and residual zinc species. Following this, the mixture was freeze-dried for 48 hours. To convert $Zn(OH)_2$ compound formed duet to the reaction of Zn^{2+} and OH^- (scheme 1) into ZnO, the samples were then dried for an hour at 120 ^oC. Based on CNC to $Zn(NO_3)_2.6H_2O$ weight ratio, the four samples are designated CNC/$ZnO_{1/4}$, CNC/$ZnO_{1/2}$, CNC/$ZnO_{3/4}$, and CNC/ZnO_1 to represent CNC/ZnO (25, 50, 75 and 100%) sample respectively.

2.6 Characterization

2.6.1 Zeta potential test

Using a Zeta sizer (Malvern Zeta Nano, ZE3600), the CNC and ZnO/CNC nanohybrids zeta potential values were determined in aqueous solution. An aqueous suspension (2.5 mg/mL) of the material, which was diluted to 0.01% was used to measure in triplicate at 25 ^oC. Table 1 displays the typical zeta potential values of CNC/ZnO nanohybrids.

2.6.2 Carboxyl content analysis

Conductometric titration is very important to determine the COOH group concentrationin the CNC/ZnO nanohybrids. 0.1g of dried sample and 10mL of 0.01M of NaCl solution were mixed with 100mL of DI water, and to produce a well-dispersed suspension, the produced solution was vigorously swirled. 0.1 M HCl was added to the mixture to reduce the pH to 2.5–3.0. 0.015 M NaOH solutions were then added to the suspension at a rate of 0.1 ml per drop, bringing the pH up to 11. From conductivity-pH curves, the sample's carboxyl group content was determined.

2.6.3. UV–Vis absorption

In the range of 200 to 800 nm, UV–Vis spectrophotometer (Perkin Elmer UV–Vis spectroscope, USA), was utilized to determine the optical properties of MB suspension. Four CNC/ZnO hybrids samples, such as CNC/$ZnO_{1/4}$, CNC/$ZnO_{1/2}$,

CNC/$ZnO_{3/4}$, and CNC/$ZnO_{3/4}$ were characterized.

2.6.4 Scanning electron microscope

The morphologies of the synthesized CNC/ZnO nanohybrids and CNC samples were evaluated by utilizing SEM (high vac. SED, PC-std, 15 kV) at 2.0 kV accelerating voltage at room temperature. Before SEM observation, the diluted suspension was added to dry on a silicon slice.

2.6.5 Fourier transform infrared spectroscopy (FTIR)

An FT-IR spectrometer was used to collect the samples' FT-IR spectra. The spectra were recorded at wave numbers range of 4000-400 cm-1. The FTIR analysis was performed using the IS50 FTIR spectrometer.

2.6.6 X-ray powder diffraction

Using monochromatic Cu Ka radiation at k = 1.54056 A in the 2 range of 5-80 at a scan rate of 5 min-1, an X-ray powder diffractometer (SHIMADZU XRD-6000) was used to analyze the crystallite size and morphology CNC/ZnO nanohybrids and CNC. The crystallinity size was calculated using the Scherrer equation (equation 3) (Yu et al. 2012). The current and tension of the X-ray generator were 30 mA and 40 kV, respectively.

2.7 Photocatalytic activity

Absorption spectroscopy under UV irradiation was used to analyze the materials' photocatalytic activity by previously reported procedures Fallah et al. (2011) and Zhai et al. (2014) depending on the photodegradation response of methylene blue (MB) dye. MB was exposed to high-intensity (365 nm, 115V-60 Hz, 2.5 A, 100 W) Lamp UV irradiation to examine CNC/ZnO nanohybrid photocatalytic properties. In 500 ml of deionized water, 10 ppm stock solution of MB was produced, and then 2 mg of different samples was added to 60 ml of 10ppm dye solution. The solution was stirred with a magnetic stirrer for 15 minutes in the dark to reach the system's adsorption equilibrium before irradiation. The mixture was exposed to UV irradiation for 15 min time intervals (15, 30, 45, and 75). The testing samples (CNC, CNC/ZnO_1, CNC/$ZnO_{3/4}$, CNC/$ZnO_{1/2}$, and CNC/$ZnO_{1/4}$) were removed from the colloidal mixture, and cleaned supernatant was obtained by centrifuging for 15 minutes at 5,000 rpm. The Perkin Elmer UV-Vis spectroscope (USA) was then utilized to determine the absorbance spectra of the supernatant from 350 to 850 nm wavelength. The absorbance value at 660 nm was used to calculate the dye concentration during the degradation process. To calculate the percentage of MB degradation, the equation below was used.

Degradation rate = ……. (1)

Where: C_t and C_0 are the concentrations of the MB after and before UV radiation, respectively.

2.8 Antioxidant activities

The DPPH radical scavenging assay described by Blois (1958) and Desmarchelier et al. (1997) was used to examine the antioxidant potential of samples to scavenge free radicals. The color change of a methanolic solution of 2, 2-diphenyl-1-picrylhydrazyl (DPPH) was utilized to assess the potential scavenging activities of free radicals of the CNC/ZnO samples. When DPPH is dissolved in methanol, it generates a violet or purple color, with antioxidants' actions cause to fade to various shades of yellow color. In order to investigate the antioxidant properties of the prepared sample,

Ascorbic acid was utilized as a standard to measure the percentage of DPPH radical scavenging activity using equation 2. A 0.1 mM DPPH solution in methanol was initially dissolved. Subsequently, 2.4 mL of this solution was added to 1.6

mL of CNC/ZnO nanohybrid sample dissolved in methanol at various concentrations (25 - 125 g/mL). After fully vortexing the mixed solution, the reaction mixture was kept at room temperature for 30 minutes. At 517 nm, the mixture's absorbance was determined spectrophotometrically.

% DPPH radical scavenging activities = ……(2)

Where: A_1 and A_0 are UV absorbance of samples and control, respectively

2.9 Antibacterial susceptibility testing of sample

The in vitro bactericidal activity of CNC/ZnO_1, CNC/$ZnO_{3/4}$, CNC/$ZnO_{1/2}$, and CNC/$ZnO_{1/4}$ was investigated using the disc diffusion method. The dry samples were first dissolved in sterilized distilled water (5 mL) to achieve the necessary test concentration of 0.25, 0.50, 0.75, and 1.00 mg/ml. 5 mm-diameter discs of Whatman's No. 1 filter paper were produced using a paper borer. These discs were exposed for 24 hours to each test concentration. The discs were taken out and dried in an aseptic condition.

A pure culture of two gram -ve bacteria species such as *Klebsiella pneumonia and Escherichia coli*, and two gram +ve photogene including *Staphylococcus epidermidis and Staphylococcus aureus* were incubated for 72 hours to make the bacterial solution. The suspension was made using sterilized distilled water. Using a spectrophotometer, the suspension's optical density was adjusted to 0.132 at 600 nm. This is equivalent to 0.5 McFarland turbidity standards. At this turbidity level, 1.5 × 108 CFU/mL of bacteria is present. The Muller-Hinton Agar medium was aseptically inoculated with around 0.5 mL of the bacterial suspension, and the spreader was used to disseminate it evenly. Sensitive discs of ciprofloxacin 30 µg/mL concentration were used as standard controls. Within 15 minutes, the dried discs were applied to the inoculated Petri dishes. All the Petri plates were incubated at 37ºC. Each test concentration was examined three times during the antibacterial susceptibility testing process. The antibacterial activity of extracts was assessed using the zone of inhibition's diameter. Using a transparent ruler or meter, the inhibitory zone was seen and measured in millimeters.

2.10 Statically analysis

Origin 8 software was used to analyze the results variance (one-way ANOVA). All measurements were done three times (n=3), and the results are the average of three repetitions with standard deviations (SD). A confidence limit of P value less than or equal to 0.05 was used to determine significance.

3. Result And Discussion

3.1 Size distribution, carboxyl content, and zeta potential

The DLS experiment was performed on a CNC/ZnO suspension made from CNC. The resulting size distribution is shown in Table 1. It was found that the CNC sample had the shortest average particle size (94.2 - 259 nm) than CNC/$ZnO_{1/4}$ (103.4 - 281 nm), CNC/$ZnO_{1/2,}$ (122.4- 295.3 nm), CNC/$ZnO_{3/4}$ (128.4-301.4 nm) and CNC/ZnO_1 (119 to 341.2 nm) samples. This finding indicates that hydrolysis of COA by CAA is more likely to produce smaller size cellulose nanocrystals. However, the size of the samples increased as ZnO nanoparticles were added to CNC. CNC/ZnO_1 samples displayed the biggest size compared to the other samples. Since more ZnO nanoparticles grow on the CNC surface due to more Zn^{2+} being coupled with CNC. As shown in Table 1, the size of CNC/ZnO samples slightly increased in the order of CNC, CNC/$ZnO_{1/4}$, CNC/$ZnO_{1/2}$, CNC/$ZnO_{3/4}$ and CNC/ZnO_1 with the size distribution of 94.2 - 259 nm, 103.4 - 281 nm, 122.4- 295.3 nm, 128.4- 301.4 nm, and 1119 to 341.2 nm respectively.

The results of the carboxyl group content of the CNC/ZnO nanohybrid obtained based on the *conductometric titration* method are shown in Table 1. The highest concentration was found for CNC samples (0.75± 0.08mmol/g) due to more carboxyl groups. The carboxyl content of the CNC/ZnO_1 showed the smallest amount (0.15± 0.24) than CNC/$ZnO_{3/4}$(0.37± 1.01), CNC/$ZnO_{1/2}$ (0.58±0.78) and CNC/$ZnO_{1/4}$ (0.71± 2.01). This is due to more hydroxyl groups in CNC enclosed by ZnO nanoparticles. When the concentration of Zn^{2+} increased, the reaction solution contained many Zn^{2+} ions and reacted with more hydroxyl groups of the dissolved CNC, this characteristic decreased the carboxyl content.

The average value of zeta potential acquired for CNC, CNC/$ZnO_{1/4}$, CNC/$ZnO_{1/2}$, CNC/$ZnO_{3/4}$, and CNC/ZnO_1 was -33mV, -13.7mV,-11.7mV, -10.4mV and -9.25mV, respectively (Table 1). All CNC/ZnO samples exhibited lower zeta potential compared to CNC. This is due to the carboxyl group found in CNC participating in the ZnO nanoparticles preparation system. During the preparation of CNC via esterification reaction, negatively charged nanoparticles are produced due to carboxyl groups on their surface. This affects the tendency of the zeta potential value of the CNC sample (Yu et al. 2016). CNC/ZnO_1 has the lowest absolute value of zeta potential (-9.25 Mv), followed by CNC/$ZnO_{3/4}$ with a value of -10.4 Mv. However, CNC/$ZnO_{1/4}$ has the highest value (-13.7 Mv) among the four nanohybrid samples. This is because the zeta potential of the CNC is consistent with the carboxyl content of CNC samples (Table 1). As the content of COOH increases, the absolute value of zeta potential also increases(Yu et al. 2016). CNC had the highest absolute zeta potential (-33 mV), indicating the highest repelling force between CNC samples driven by the most considerable carboxyl content.

Table 1 zeta potential, carboxyl content, and size distribution of CNC/ZnO nanohybrids

Samples	Zeta potential	Carboxyl content	Size (d.nm) from DLS data
CNC	-33 mV	0.75± 0.19[a]	94.2 - 259 nm
CNC/$ZnO_{1/4}$	-13.7 mV	0.71± 2.01[b]	103.4 - 281 nm
CNC/$ZnO_{1/2}$	-11.7 mV	0.58± 0.78[c]	122.4- 295.3 nm
CNC/$ZnO_{3/4}$	-10.4 mV	0.37± 1.01[d]	128.4- 301.4 nm
CNC/ZnO_1	-9.25 mV	0.15± 0.24[e]	1119 to 341.2 nm

All data were examined in triplicate, and the mean value ± SD *was taken and written in the table. The identical alphabetical letter indicates that there are no statically significantly different (P>0.05) between values in the same column.*

3.2 Scanning Electron Microscope (SEM) Analysis

Fig. 3 displays ROA, COA, CNC, and CNC/ZnO samples in SEM images. The SEM image shows the differences in the fiber surfaces between ROA and COA by observing images after and before the bleaching process. The image confirmed that the surface of COA fibers is smoother and has less solid aggregate than ROA fiber. Additionally, the COA exhibit decreased aggregation, suggesting that the bleaching procedure was successful in removing a sizable portion of the amorphous mass from the fiber surfaces, such as low molar mass polysaccharides, impurities, and lignin reported previously by César et al. (2015); Khan et al. (2009) and Gültekin (2016). ROA showed a larger size (23.0 to 8.34 µm) than COA (18.05 to 4.01µm) samples. SEM images of ZnO/CNC and CNC show that the morphology of CNC is similar to a rod-shaped size with a smaller size (31 to 259 nm) due to the acid hydrolysis influence of chemicals in the synthesis

process. Following the precipitation of CNC and Zn^{2+} ions in the CNC/$ZnO_{1/2}$ sample, ZnO nanoparticles with a mean diameter of 164.18 nm and size distribution of 94–259 nm were formed on the surface of CNC. The average diameter of ZnO nanoparticles increased to 183.5 nm in a CNC/ZnO_1 sample with a size range of 128 to 351 nm due to an increase in Zn^{2+} ion concentration. As more Zn^{2+} ions become immobilized on the CNC surface, causes the number of ZnO particles in CNC increases.

3.3 X-ray powder diffraction (*XRD*)

Fig. 4 displays the CNC and CNC/ZnO nanohybrid's XRD image. The cellulose I characteristic peaks are visible in the CNC's XRD pattern at 2θ = 15.68°, 22.58°, and 34.54° (French AD 2014). In addition to the cellulose-specific peaks, The ZnO/CNC samples also show additional peaks at 69.42°, 67.5°, 62.54°, 56.76°, 47.68°, 36.38°, 34.52°, and 31.98°, which are assigned to the values (201), (112), (103), (110), (102), (101), (002), and (100), respectively (Sirvio¨ JA et al. 2014; Ul-Islam et al. 2014). This is an indication of the formation of nanohybrids. The crystal structure of the ZnO is revealed by the prominent intensity diffraction peaks in the XRD scheme (Sharma et al. 2019; Guan et al. 2019). Fig. 4 shows two-phase structures that show CNC/ZnO (#) and CNC (*) were observed. This showing using CNC, ZnO nanohybrid has been synthesized effectively. The low-intensity peaks of CNC/ZnO nanohybrids compared to the XRD peak of pure ZnO nanoparticles showed the deposition of ZnO NPs on the CNC surface. The findings further demonstrate that the existence of ZnO crystals does not affect the cellulose crystal structure. Three CNC/ZnO nanohybrid samples have similar XRD patterns. This demonstrated the efficient one-step ZnO synthesis on CNC in a successful manner. These profiles indicated that the presence of well-crystalline ZnO has not changed the crystal structure of the cellulose matrix. The Figure further demonstrated that, with rising Zn^{2+} ion concentrations, ZnO peaks get broader and more powerful over time. This suggests that the CNC/ZnO nanohybrids' crystal size and crystallinity have increased. Using debye-Scherrer technology, the crystal size (D) of the CNC/ZnO and CNC, structures were determined from the XRD data using equation (3).

$$D_{hkl} = \frac{k\lambda}{\beta(\frac{\pi}{180})cos\theta} \quad \text{.....(3)}$$

Where: β is the integral breadth of the maximum complete width (FWHM), λ is X-ray radiation's wavelength (k=0.94), D_{hkl} is the size of a crystallite in nanometers as viewed from the crystal's(hkl) plane, (π/180) is the correction factor in changing β into radians, and θ is the scattering angle,

The predicted size of the CNC hybrid's ZnO crystal was 11.5nm, 10.7nm, and 9.8nm for CNC/ZnO_1, CNC/$ZnO_{3/4,}$ and CNC/$ZnO_{1/2}$, respectively. The three samples' estimated crystallite sizes match those in Fig. 4 XRD patterns because the purer ZnO is typically associated with larger crystal sizes, which are typically associated with sharper intensity peaks., In contrast, the CNC/ZnO spectrum's smaller and wider peaks are connected to a smaller crystal size (Mumalo-Djokic et al. 2008; Taunk et al., 2015). These intensity peaks and crystal planes showed that ZnO nanoparticles effectively formed on the CNC surface.

3.4 Ultraviolet-visible (UV-Vis)

The optical properties of CNC/ZnO nanohybrids with various Zn^{2+} concentrations were examined by utilizing a UV-Vis spectrophotometer. Fig. 5 shows the UV-Vis absorption peak of the CNC and CNC/ZnO nanohybrids. It was found that the CNC's spectra lacked any noticeable peaks between 300 and 700 nm. However, the UV–Vis peak showed a strong peak before 400 nm for all ZnO/CNC samples. The absorption bands for the CNC/$ZnO_{1/4}$, CNC/$ZnO_{1/2}$, CNC/$ZnO_{3/4}$, and CNC/ZnO_1 samples were 363, 366, 372, and 376 nm, respectively. ZnO's basic band gap absorption, which happens

when an electron transitions from the valence band to the conduction band (O2p → Zn3d), is responsible for these peaks (Zak et al. 2011). This shows that ZnO nanoparticles have formed on the surface of CNC. It is intriguing to observe that the larger ZnO caused the absorption band to move toward the red (redshift). This suggests that when the Zn^{2+} ion concentration increases, more significant ZnO nanoparticles might be produced. According to the plot of Tauc shown in Fig. 5(b), the band gaps for the samples CNC/$ZnO_{1/4}$, CNC/$ZnO_{1/2}$, CNC/$ZnO_{3/4}$, and CNC/ZnO_1 are 3.32, 3.29, 3.21, and 3.07 eV, respectively. The sample band gaps estimated from (αh)2 versus (h) plot match with the mode of Kubelka-Munk (Yu et al. 2008).

3.5 Fourier transform infrared spectroscopy (FTIR)

The identification of functional group and bond structure determination of the CNC/ZnO nanohybrids samples was examined by FTIR instrument in the peak range of 400 and 4000 cm-1 (Fig. 6). Peaks at 3315-3340 cm-1 in the CNC/ZnO nanohybrids and CNC spectra were attributed to the O-H stretching mode (Azizi et al. 2013). After adding ZnO to cellulose, the strength of the O-H stretching vibrations weakened for CNC/$ZnO_{3/4}$ and CNC/ZnO_1, as shown in Fig. 6. This suggests oxygen atoms participated in the bonding interaction with ZnO and weakened the O-H bond. The peak at 1435 cm-1 was assigned to the CH2 vibration and taken as the crystallization band for each cellulose material, while sharp peak was indicated to C-O stretching for the CNC and CNC/ZnO samples. Its intensity decreases as the concentration of ZnO increases. According to Lu and Hsieh (2010), the peak at 1,650 cm^{-1} is because of the C-O-C bond stretching of glucose and pyranose ring skeletal vibration, but the peak at roughly 1,065 cm^{-1} is caused by the O-H bending of a water molecule (Cherian et al. 2008). The band intensity (1.721cm^{-1}) for the C=O stretch decreased in intensity compared to the CNC peak intensity. This resulted from the potent interaction between the COOH groups on the CNC surface and the ZnO NPs.

Compared to CNC, more absorption peaks at 600–400 cm were found in ZnO/CNC nanohybrids, and these peaks were linked to Zn–O stretching modes (Azizi et al. 2013; Wei et al. 2013). The Zn-O peaks of ZnO/CNC_1, ZnO/$CNC_{3/2}$, and ZnO/$CNC_{1/2}$ were located at 435, 432, and 412 cm-1, respectively. This verifying ZnO was successfully synthesized on the CNC template (Azizi et al. 2013; Zhang et al. 2013). The lack of a peak in the CNC sample between 400 and 450 cm-1 indicates that ZnO is not present in the sample. With increasing Zn^{2+} ion concentration, a little shift of the Zn-O stretching bands to higher wavenumbers was observed because of the lattice structure of the ZnO nanoparticles. The absorption peak at 2900 cm^{-1}, is related to the C-H vibration of sp3-hybridized carbon. This peak vanished when the CNC/ZnO nanohybrid was synthesized (Oyewo et al. 2019). This peak's intensity also decreased with ZnO loading increase (Fig. 6). The decrease in intensity of the peak indicates that ZnO is present or loaded to the CNC lattice. A similar observation was made in the work of Ali et al. (2016) and Keshk and Hamdy (2019) using nanocomposites made of cellulose and ZnO.

3.6 Application of CNC/ZnO nanohybrids

3.6.1 Photocatalytic activity

By using solid-phase photodegradation MB dye, the photocatalytic activity of four different samples, including CNC/ZnO_1, CNC/$ZnO_{3/4}$, CNC/$ZnO_{1/2}$, and CNC/$ZnO_{1/4}$ (Fig. 7), was investigated. The degradation of MB caused by exposure to UV radiation was used to determine the effectiveness of CNC/ZnO samples as photo-catalyst activities. The adsorption-desorption studies were carried out in complete darkness for 5 minutes, and the absorption spectra after this adsorption-desorption step are reported as "0 min". At various time intervals and under the identical circumstances, the photocatalytic activity of CNC was also assessed for comparison.

To determine how much UV light could potentially degrade MB, a blank test was run to see how much MB would degrade without a photocatalyst.

Fig. 7a, 7b, and 7c illustrate the photocatalytic capability of CNC/ZnO nanohybrids to degrade MBs when exposed to UV light in a 75-minute irradiation time. The result showed that in samples containing CNC solely, no notable changes in the UV absorption band of MB were seen after 75 minutes of UV exposure. Fig. 7d shows the MB degradation when it reacted with different CNC/ZnO samples. The degradation increase in the order of CNC/ZnO_1, CNC/$ZnO_{3/4}$, CNC/$ZnO_{1/2}$, and CNC/$ZnO_{1/4}$. The Fig. also shows that there is no significant difference in absorbance between CNC and MB; this showed that CNC has the lowest capacity to reduce the absorbance of MB. Fig. 7d also shows the MB's absorbance reduction due to the addition of CNC and CNC/ZnO samples. Based on the Fig.s, the absorption peak of MB (2.23) reduced to 0.79, 0.93, 1.07, and 1.38 for CNC/ZnO_1, CNC/$ZnO_{3/4}$, CNC/$ZnO_{1/2}$, and CNC/$ZnO_{1/4}$ respectively. Less MB degradation was evident with higher UV absorption values. The lowest absorption peak (highest degradation) is shown in CNC/ZnO_1 and the most significant (lowest degradation) is shown in CNC/$ZnO_{1/4}$. This is related to the concentration of ZnO concentration present in the sample. As the amount of ZnO increases, the chance of e^- and h^+ reacting with O_2 and H_2O to generate free radical(OH^-) and O_2^- also increases (Fig. 9); this might take part in the direct oxidative breakdown of MB dye (Qi et al. 2017; Lefatshe et al. 2017; Balcha et al. 2016).

As seen in Fig. 8, the samples' exposure period to UV light impacts MB deterioration. To measure the effect of MB degradation with time, we measured the UV absorbance of the samples every 15-minute interval for 75 minutes. The result showed that the samples' absorbance decreased when the reaction time increased—however, the rate of degradation over time increased. As shown in Fig. 8, CNC/ZnO_1 has the highest degradation rate, while CNC/$ZnO_{1/4}$ has the lowest degradation rate every 15, 30, 45, 60, and 75 minutes of exposure to UV irradiation.

Fig. 8b demonstrate that, after 75 min of UV irradiation, ungraded MB for CNC/ZnO_1, CNC/$ZnO_{3/4}$, CNC/$ZnO_{1/2}$, CNC/$ZnO_{1/4}$ and CNC samples were 8.48, 19.65, 36.42, 45.88 and 83.48% respectively. Since ZnO was absent from the CNC sample, the 75-minute UV exposure exhibited no appreciable impact on the MB UV absorption band. After a 75-minute reaction, the lowest percentage of MB degradation (16.52%) was found in CNC, which had a lower degradation rate than CNC/ZnO_1 (91.52%), CNC/$ZnO_{3/4}$ (80.348%), CNC/$ZnO_{1/2}$ (63.58%), and CNC/$ZnO_{1/4}$ (54.12%) (Fig. 8a). According to the Figure after being exposed to UV radiation for 75 minutes in CNC/ZnO_1 nanohybrid, roughly 91.52% of the MB dye rapidly decomposed. This finding suggests that ZnO/CNC_1 nanohybrids have strong electrical interactions with ZnO nanoparticles that are well dispersed on the CNC surface. These characteristics possessed the sample to have higher photocatalytic activity than other samples. This photocatalytic performance in the present study was more effective than the photocatalytic activity (less than 90%) of CNC/ZnO nanohybrids made by Nang An et al. (2020) in 75 minutes of UV exposure time and comparable photocatalytic activities (about 90%) have been seen in the work of Yu et al. (2015) in 75 minute time.

Fig. 9 illustrates a potential mechanism for the CNC/ZnO nanohybrids photocatalytic activity according to the above results. ZnO can make photogenerated electron-hole pairs by absorbing UV light. The resulting photogenerated hole (h+) and electron (e-) could go to the ZnO nanoparticles' surface, interacting with both H_2O and O_2that have been absorbed on the surface of ZnO to produce O_2- and OH, which could take part in the direct oxidation that leads to dye degradation (Huang et al. 2014; Zhai et al. 2014).

3.6.2 Determination of antioxidant activity Using the DPPH radical scavenging method

As a result of its sensitivity to detect active substances at low doses, the 2,2-Diphenyl-1-picrylhydrazyl (DPPH) assay is frequently employed to test for antioxidant activity (Tettey and Shin 2019). Since DPPH is a nitrogen-centered free

radical, any substance significantly reducing DPPH levels may also lower the amount of other reactive nitrogen species (Tettey and Shin 2019). Our findings show that the CNC/ZnO nanohybrid could dose-dependently quench DPPH free radicals at 25, 50, 75, 100, and 125 g/ml concentrations. According to the data in Table 2, CNC/ZnO_1 had the highest percentage inhibition value (25 g/mL, 11.09% 1.21; 50 g/mL, 21.43% 2.11; 75 g/mL, 32.07% 0.74; 100 g/mL, 42.51% 0.62; and 125 g/mL, 53.15% 1.03) than the other samples. This demonstrated that it had higher free radical scavenging activity levels than the other samples. CNC/ZnO_1 has not shown a significant (p percentage inhibition compared to CNC/$ZnO_{3/4}$. However, there is a significant (p percentage inhibition value in the rest of the samples. CNC's value is the smallest compared to CNC/ZnO_1, CNC/$ZnO_{3/4}$, CNC/$ZnO_{1/2,}$ and CNC/$ZnO_{1/4}$ samples. This is an indication that CNC has the smallest antioxidant activities. All samples in table 2 showed a much lower percentage inhibition value than that of the AA standard (125 µg/ml, 93.75 %±0.11).

Table 2 Percentage inhibition of different CNC/ZnO samples

Samples	Concentration ration (µg/ml)				
	25	50	75	100	125
CNC/ZnO_1	11.09±1.21^a	21.43±2.11^a	32.07±0.74^a	42.51±0.62^a	53.15±1.03^a
CNC/$ZnO_{3/4}$	10.78±1.31^a	21.21±1.91^a	31.73±0.91^a	42.06±0.57^a	52.58±0.65^a
CNC/$ZnO_{1/2}$	9.10±0.45^b	17.73±0.34^b	26.48±0.34^b	35.33±0.56^b	44.08±0.34^b
CNC/$ZnO_{1/4}$	6.22±0.26^c	12.25±1.45^c	18.17±2.45^c	24.30±0.54^c	30.12±0.76^c
CNC	1.21±0.23^d	2.31±0.43^d	3.41±0.19^d	4.51±0.27^d	5.61±0.39^d
AA	51.15±0.65^e	62.42±2.34^e	74.53±0.97^e	80.61±0.32^e	93.75±0.11^e

All data were examined in triplicate, and the mean value ± SD *was taken and written in the table. The identical alphabetical letter indicates that there are no statically significantly different (P>0.05) between values in the same column. AA= ascorbic acid*

The IC50 values of CNC/ZnO samples are presented in Fig. 10. Their value ranged from 117.66 ± 2.07µg/ml to 554.30 ± 2.07µg /ml. All CNC/ZnO samples had IC50 values that were greater (P < 0.05) than ascorbic acid, indicating that they are the least effective in scavenging DPPH radicals compared to standards. CNC samples without ZnO have the largest (554.30± 2.11), and AA has the lowest (19.30 ±1.03) IC50 value. There is no significant (P > 0.05) IC50 value difference between CNC/ZnO_1 and CNC/$ZnO_{3/4}$ samples. Since the antioxidant activities and IC50 value have inversely proportional values, the results showed that CNC had the lowest antioxidant activities, whereas CNC/ZnO_1 had the highest antioxidant activities.

The results from both % inhibition and IC50 values demonstrated that when Zn^{2+} concentrations increase, the antioxidant activities of the samples to scavenge free radicals also increase. As ZnO nanoparticle concentrations rise, more DPPH free radicals are quenched. This results in to increase the antioxidant activities. Similar work was done by Ali et al. (2016). Their work showed that ZnO-Cellulose showed lower DPPH free radical scavenging activities (14.85%) than the present work. The study also revealed that DPPH scavenging activity was shown to rise with a rise in nanoparticle concentrations. This characteristic is also observed in this work.

3.6.3 Antibacterial activities

The lack of antibacterial activities in cellulose may restrict its usage in biomedical and environmental applications. This is why researchers are initiated to synthesize zinc nanocomposites with cellulose for antibacterial activities (Azizi et al. 2014; Ul-Islam et al. 2014). By converging cellulose into CNC and preparing CNC/ZnO. We made cellulose to have antibacterial activities (Fig. 11).

In this study, gram-negative bacteria species such as *Escherichia coli* and *Klebsiella pneumonia*, as well as gram-positive bacteria including *Staphylococcus aureus* and *Staphylococcus epidermidis*, were used to investigate the antibacterial efficacy of the CNC/ZnO nanohybrids. The CNC was used as a control sample. The Ciprofloxacin drug was employed as a standard sample in the Agar well diffusion method to examine the antibacterial activity.

The disc diffusion method was used to assess the antibacterial activity. It was shown that the inhibition zones produced by CNC/ZnO nanohybrids against *Escherichia coli* and *Klebsiella pneumonia* ranged from 32.33 2.51 to 41.33 1.15 and 31.66 3.51 to 41.00 1, respectively*. For gram-positive bacteria species such as Staphylococcus aureus and Staphylococcus epidermidis,* zone inhibition was observed in the range of 26.00±1.00 to 40.33±2.08 and 31.22±1.52 to 38.66±1.15 respectively. The standard drug in this investigation, Ciprofloxacin, demonstrated a 30 00±0.00 zone of inhibition for testing four bacterial species.

The size of the growth-inhibiting ring used to combat *Staphylococcus aureus against four different samples such as* $CNC/ZnO_{1/4}$, $CNC/ZnO_{1/2}$, $CNC/ZnO_{3/4,}$ and CNC/ZnO_1 were 26.00± 1.00, 32.33± 2.51, 33.33± 2.88, and 40.33± 2.08 mm, respectively. This showed that as the concentration of Zn^{2+} increases, the antibacterial activities of *Staphylococcus aureus also increase. However, this uniform trend is not observed for the other three bacteria species, such as Escherichia coli, Klebsiella pneumonia, and Staphylococcus epidermidis (Fig. 11). There was no significant difference (P in the value of disc diffusion between Escherichia coli* and *Klebsiella pneumonia, almost in all concentrations. This showed that the antibacterial properties between these two species are almost the same.* The inhibition zone of CNC/ZnO_1 (16.3±3.21mm), $CNC/ZnO_{3/4}$ (17.3±2.51 mm), $CNC/ZnO_{1/2}$ (17.3±2.51 mm), and $CNC/ZnO_{1/4}$ (17.3±2.51 mm) against *Escherichia coli* and the inhibition zone of CNC/ZnO_1 (16.3±3.21mm), $CNC/ZnO_{3/4}$ (17.3±2.51 mm), $CNC/ZnO_{1/2}$ (17.3±2.51 mm) and $CNC/ZnO_{1/4}$ (17.3±2.51 mm) against *Klebsiella pneumonia* were statistically significant ($P<0.05$) greater than inhibition zone of the corresponding samples of gram-positive bacteria species such as *Staphylococcus aureus* and *Staphylococcus epidermidis*. This showed that gram-negative bacteria respond more positively to antibacterial activities than gram-positive bacteria species. *Escherichia coli* and *Klebsiella pneumonia*, there was no statistically significant ($P < 0.05$) difference among the inhibition zone of CNC/ZnO_1, $CNC/ZnO_{3/4,}$ and $CNC/ZnO_{1/4}$. However, in *Staphylococcus aureus* and *Staphylococcus epidermidis* there was a statistically significant ($P < 0.05$) difference among inhibition zone against CNC/ZnO_1, $CNC/ZnO_{3/4}$, $CNC/ZnO_{1/2}$ and $CNC/ZnO_{1/4}$.

The inhibition zone of the standard drug Ciprofloxacin (30.00 ± 1.00) exhibited the lowest value except for the value of CNC/ZnO_1 against *Staphylococcus aureus* (26.00± 1.00). This showed that the synthesized CNC/ZnO samples have high antibacterial activities. The data in table 3 showed that as the concentration of ZnO nanohybrids increased, the % inhibition of the samples also increased. This showed that antibacterial activities are directly dependent on concentration.

The use of CNC/ZnO nanohybrids against *Staphylococcus aureus* and *Escherichia coli* has been reported by Abdalkarim et al. (2018b) to inhibit the growth of bacteria and reduce bacterial counts. Despite using diluted nanocomposites, their findings indicated that the bacteria were inhibited in 4.5 and 3mm zones, respectively. This value is too small compared to our work. In another similar work by Abdalkarim et al. (2018a), zones of inhibition for the antibacterial activity of CNC/ZnO nanohybrids against *Staphylococcus aureus* and *Escherichia coli* were also observed to be 3.0 to 5.1 mm and 4.1 to 4.9 mm, respectively. This value is also small compared to our value. Yu et al. (2015) discovered effective CNC/ZnO nanohybrid antibacterial activity against *Staphylococcus aureus* and *Escherichia coli*, with the diameter of the

growth inhibition ring measuring 4.5 and 4.3 mm, respectively. This value is also too small compared to the value found in our work (Fig. 11).

Due to the greater surface area of ZnO nanostructures, more ROS are produced. The bacteria become oxidized by the metal component, which renders their proteins inactive, decreases cell permeability, and finally results in their death. The generated ROS may penetrate and directly damage bacteria's cell walls, causing peroxidation of the organism's PUFA phospholipids and bacterial death (Wang et al. 2017; Sawai et al. 1996). Additionally, another bactericidal mechanism might result from electromagnetic interaction between the pathogen and the nanoparticles, which would halt the bacteria's activity (Mohd Yusof et al. 2019).

Table 3 The zone of inhibition that CNC/ZnO showed against four bacteria pathogens such as *Staphylococcus epidermidis, Staphylococcus aureus, Escherichia coli,* and *Klebsiella pneumonia,*

Bacteria species	Trial	Samples				Ciprofloxacin (standard)
		CNC/ZnO_1	$CNC/ZnO_{3/4}$	$CNC/ZnO_{1/2}$	$CNC/ZnO_{1/4}$	30.00± 00
Escherichia coli (-ve)	1st	30	42	40	42	
	2nd	32	40	40	40	
	3rd	35	41	42	42	
	Average	32.33 ± 2.51[a]	41± 1.00[b]	40.66 ± 1.15[b]	41.33± 1.15[b]	
Klebsiella pneumonia *(-ve)*	1st	28	38	43	40	30.00± 00
	2nd	35	40	45	41	
	3rd	32	41	40	42	
	Average	31.66± 3.51[a]	39.66± 1.52[b]	42.66± 2.51[b]	41.00± 1.00[b]	
Staphylococcus aureus *(+ve)*	1st	25	30	30	38	30.00± 00
	2nd	27	35	35	42	
	3rd	26	32	35	41	
	Average	26.00± 1.00[a]	32.33± 2.51[b]	33.33± 2.88[b]	40.33± 2.08[c]	
Staphylococcus epidermidis	1st	33	32	38	38	30.00± 00
	2nd	30	30	35	40	
	3rd	31	30	38	38	
	Average	31.22± 1.52[a]	30.66± 1.15[a]	37± 1.73[b]	38.66± 1.15[b]	

Conclusion

This research study synthesized CNC/ZnO through a simple and single-stage process. Data from SEM, XRD, DLS, and FTIR spectra showed that ZnO nanoparticles were loaded on carboxylated CNC to form a nanohybrid of CNC/ZnO with a mean size of 164.18 nm in the range between 94–351 nm. ZnONPsare distributed around the CNC because of the electrostatic interaction between the Zn^{2+} ion and the carboxyl group of the CNC. The synthesized CNC/ZnO nanohybrids showed high photocatalytic activities, with a 90% degradation rate of MB. The nanohybrid samples also showed higher antibacterial than CNC. All the samples exhibited high antibacterial activities against both grams positive (*Klebsiellapneumonia and Escherichia coli*) and gram-negative bacteria (*Staphylococcus epidermidis and Staphylococcus aureus)* with inhibition zone in the range of26.00±1.00 to 41.33± 1.15 mm compared to Ciprofloxacin. The result also showed that CNC/ZnO nanohybrids have higher antioxidant activities than CNC. In the CNC sample, the lowest DPPH radical scavenging activities, 5.61±0.39, were observed. The highest % inhibition of DPPH (53.15±1.03%) and the lowest IC50 value (117.66μm/ml) were observed in CNC/ZnO_1 sample. The above data showed that ZnO/CNC nanohybrid could be applied in dye removal, wastewater treatment, and antibacterial activity. ZnO/CNC nanohybrid showed weaker antioxidant activity in this study, necessitating further study in this area.

Declarations

Acknowledgments

The Department of Industrial Chemistry at Addis Ababa Science and Technology University provided the opportunity for the authors to conduct this research. The only Doctoral Dissertation Research provided by Addis Ababa Science and Technology University, Ethiopia, was used.

Ethical approval

Not applicable

Competing interests

The authors declare no competing interests

Authors contributions

All authors contributed to the study conception and design. Material preparation, data collection and analysis were performed by Limenew Abate Worku. The first draft of the manuscript was written by Rakesh Kumar Bachheti and Mesfin Getachew Tadesse. Archana Bachheti prepare different table and figures. All authors commented on previous versions of the manuscript. All authors read and approved the final manuscript. All authors also worked on revision of the article.

Data availability

All data generated or analyzed during this study are included in this paper

Funding

This study was financially supported by Addis Ababa science and Technology University. No external funding available

References

1. Abdalkarim SYH, Yu HY, Wang C, Huang LX, Yao J (2018) Green synthesis of sheet-like cellulose nanocrystal–zinc oxide nanohybrids with multifunctional performance through one-step hydrothermal method. *Cellulose* 25(11):6433-6446.
2. Abdalkarim SYH, Yu HY, Wang C, Yang L, Guan Y, Huang L, Yao J (2018) Sheet-like cellulose nanocrystal-ZnO nanohybrids as multifunctional reinforcing agents in biopolyester composite nanofibers with ultrahigh UV-shielding and antibacterial performances. *ACS Applied Bio Material* .1(3):714-727.
3. Abouzeid RE, Khiari R, El-Wakil N, Dufresne A (2018) Current state and new trends in the use of cellulose nanomaterials for wastewater treatment. *Biomacromolecules* 20(2):573-597.
4. Ali A, Ambreen S, Maqbool Q, Naz S, Shams MF, Ahmad M, Phull AR, Zia M: Zinc impregnated cellulose nanocomposites (2016) Synthesis, characterization and applications. *J Phys Chem Solids* 98:174-182.
5. Ambawu T (2019) Value chain analysis of groundnut in Pawi woreda, Metekel Zone, Ethiopia, https://www.grin.com/document/505489.
6. Azizi S, Ahmad M, Mahdavi M, Abdolmohammadi S (2013) Preparation, Characterization, and Antimicrobial Activities of ZnO Nanoparticles/Cellulose Nanocrystal Nanocomposites. *BioResources* 8(2).
7. Azizi S, Ahmad MB, Ibrahim NA, Hussein MZ, Namvar F (2014) Cellulose nanocrystals/ZnO as a bifunctional reinforcing nanocomposite for poly (vinyl alcohol)/chitosan blend films: fabrication, characterization and properties. *Int J Mol Sci* 15(6):11040-11053.
8. Balcha A, Yadav OP, Dey T (2016) Photocatalytic degradation of methylene blue dye by zinc oxide nanoparticles obtained from precipitation and sol-gel methods. *Environ Sci Pollut Res* 23(24):25485-25493.
9. Blois MS (1958) Antioxidant determinations by the use of a stable free radical. *Nature* 181(4617):1199-1200.
10. César N, Pereira-da-Silva M, Botaro V, Menezes A (2015) Cellulose nanocrystals from natural fiber of the macrophyte Typha domingensis: extraction and characterization. *Cellulose* 22(1):449-460.
11. Chen W, Yu H, Lee SY, Wei T, Li J, Fan Z (2018) Nanocellulose: a promising nanomaterial for advanced electrochemical energy storage. *Chem Soc Rev* 47(8):2837-2872.
12. Cherian BM, Pothan LA, Nguyen-Chung T, Mennig Gn, Kottaisamy M, Thomas S (2008) A novel method for the synthesis of cellulose nanofibril whiskers from banana fibers and characterization. *J Agric Food Chem.* 56(14):5617-5627.
13. Clarkson CM, El Awad Azrak SM, Forti ES, Schueneman GT, Moon RJ, Youngblood JP (2021) Recent developments in cellulose nanomaterial composites. *Adv Mater* 33(28):2000718.
14. Desmarchelier C, Novoa Bermudez M, Coussio J, Ciccia G, Boveris A (1997) Antioxidant and prooxidant activities in aqueous extracts of Argentine plants. *Int J Pharmacogn Phytochem* 35(2):116-120.
15. Dong YD, Zhang H, Zhong GJ, Yao G, Lai B (2021) Cellulose/carbon composites and their applications in water treatment–a review. *J Chem Eng.* 405:126980.
16. Du H, Liu W, Zhang M, Si C, Zhang X, Li B (2019) Cellulose nanocrystals and cellulose nanofibrils based hydrogels for biomedical applications. *Carbohydr Polym* 209:130-144.
17. Fallah MH, Fallah SA, Zanjanchi MA (2011) Synthesis and Characterization of Nano-sized Zinc Oxide Coating on Cellulosic Fibers: Photoactivity and Flame-retardancy Study. *Chin J Chem* 29(6):1239-1245.
18. French AD (2014) Idealized powder diffraction patterns for cellulose polymorphs. *Cellulose* 21:885–896.
19. Guan Y, Yu HY, Abdalkarim SYH, Wang C, Tang F, Marek J, Chen WL, Militky J, Yao JM (2019) Green one-step synthesis of ZnO/cellulose nanocrystal hybrids with modulated morphologies and superfast absorption of cationic dyes. *Int J Biol Macromol* 132:51-62.
20. Gültekin B (2016) Bleaching of SeaCell(r) active fabrics with hydrogen peroxide. *Fibers Polym* 17(8):1175-1180.

21. Håkansson KM, Fall AB, Lundell F, Yu S, Krywka C, Roth SV, Santoro G, Kvick M, Prahl Wittberg L, Wågberg L (2014) Hydrodynamic alignment and assembly of nanofibrils resulting in strong cellulose filaments. *Nat Commun* 5(1):1-10.
22. Huang K, Li Y, Lin S, Liang C, Wang H, Ye C, Wang Y, Zhang R, Fan D, Yang H (2014) A facile route to reduced graphene oxide–zinc oxide nanorod composites with enhanced photocatalytic activity. *Powder Technol* 257:113-119.
23. Hubbe MA, Tayeb P, Joyce M, Tyagi P, Kehoe M, Dimic-Misic K, Pal L (2017) Rheology of nanocellulose-rich aqueous suspensions: a review. *BioResources* 12(4):9556-9661.
24. IUCN (1989) Policy Statement on Research Involving Species at Risk of Extinction. In Proceedings of the 27th Meeting of IUCN Council, Gland, Switzerland, 14 June 1989. 1989.
25. Keshk SMAS, Hamdy MS (2019) Preparation and physicochemical characterization of zinc oxide/sodium cellulose composite for food packaging. *Turk J Chem* 43(1):94-105.
26. Khan G, Shaheruzzaman M, Rahman M, Razzaque S, Islam M, Alam M (2009) Surface modification of okra bast fiber and its physico-chemical characteristics. *Fibers Polym* 10(1):65-70.
27. Kim JH, Lee D, Lee YH, Chen W, Lee SY (2019) Nanocellulose for energy storage systems: beyond the limits of synthetic materials. *Adv Mater* 31(20):1804826.
28. Kołodziejczak-Radzimska A, Jesionowski T (2014) Zinc oxide—from synthesis to application: a review. *Materials* 7(4):2833-2881.
29. Kwok TT, Fogg DN, Realff MJ, Bommarius AS (2017) Applying direct yellow 11 to a modified Simons' staining assay. *Cellulose* 24(6):2367-2373.
30. Lefatshe K, Muiva CM, Kebaabetswe LP (2017) Extraction of nanocellulose and in-situ casting of ZnO/cellulose nanocomposite with enhanced photocatalytic and antibacterial activity. *Carbohydr Polym* 164:301-308.
31. Lin W, Chen D, Yong Q, Huang C, Huang S (2019) Improving enzymatic hydrolysis of acid-pretreated bamboo residues using amphiphilic surfactant derived from dehydroabietic acid. *Bioresour Technol* 293:122055.
32. Liu C, Du H, Dong L, Wang X, Zhang Y, Yu G, Li B, Mu X, Peng H, Liu H (2017) Properties of nanocelluloses and their application as rheology modifier in paper coating. *Ind Eng Chem Res* 56(29):8264-8273.
33. Lu P, Hsieh YL (2010) Preparation and properties of cellulose nanocrystals: rods, spheres, and network. *Carbohydr Polym* 82(2):329-336.
34. Miao C, Du H, Parit M, Jiang Z, Tippur HV, Zhang X, Liu Z, Li J, Wang R (2020) Superior crack initiation and growth characteristics of cellulose nanopapers. *Cellulose* 27(6):3181-3195.
35. Miruts F (2020) On-farm demonstration of improved rice (Oryza sativa L) varieties in Pawe woreda of Metekel Zone, Ethiopia. *J Biology Agriculture and Healthcare* 10:1-5.
36. Mohd Yusof H, Mohamad R, Zaidan UH, Rahman A (2019) Microbial synthesis of zinc oxide nanoparticles and their potential application as an antimicrobial agent and a feed supplement in animal industry: a review. *J Anim Sci Biotechnol.* 10(1):1-22.
37. Mumalo-Djokic D, Stern WB, Taubert A (2008) Zinc oxide/carbohydrate hybrid materials via mineralization of starch and cellulose in the strongly hydrated ionic liquid tetrabutylammonium hydroxide. *Cryst Growth Des* 8(1):330-335.
38. Nang An V, Van TT, Nhan HT, Van Hieu L (2020) Investigating methylene blue adsorption and photocatalytic activity of ZnO/CNC nanohybrids. *J Nanomater* 2020.
39. Oyewo OA, Mutesse B, Leswifi TY, Onyango MS (2019) Highly efficient removal of nickel and cadmium from water using sawdust-derived cellulose nanocrystals. *J Environ Chem Eng* 7(4):103251.
40. Qi K, Cheng B, Yu J, Ho W (2017) Review on the improvement of the photocatalytic and antibacterial activities of ZnO. *J Alloys Compd* 727:792-820.

41. Reid MS, Villalobos M, Cranston ED (2017) Benchmarking cellulose nanocrystals: from the laboratory to industrial production. *Langmuir* 33(7):1583-1598.
42. Samadi M, Zirak M, Naseri A, Khorashadizade E, Moshfegh AZ (2016) Recent progress on doped ZnO nanostructures for visible-light photocatalysis. *Thin Solid Films* 605:2-19.
43. Sawai J, Kawada E, Kanou F, Igarashi H, Hashimoto A, Kokugan T, Shimizu M (1996) Detection of active oxygen generated from ceramic powders having antibacterial activity. *J Chem Eng Jpn* 29(4):627-633.
44. Sharma PR, Sharma SK, Antoine R, Hsiao BS (2019) Efficient removal of arsenic using zinc oxide nanocrystal-decorated regenerated microfibrillated cellulose scaffolds. *ACS Sustain. Chem Eng* 7(6):6140-6151.
45. Sirvio¨ JA, Anttila AK, Pirttila A, Liimatainen H, Kilpela¨inen I, Niinima¨ki JOH (2014) Cationic wood cellulose films with high strength and bacterial anti-adhesive properties. *Cellulose* 21:3573–3583.
46. Tao H, Lavoine N, Jiang F, Tang J, Lin N (2020) Reducing end modification on cellulose nanocrystals: strategy, characterization, applications and challenges. *Nanoscale Horiz* 5(4):607-627.
47. TAPPI (2002) Standards and Suggested Methods. TAPPI Press, Atlanta, Georgia, USA 2002.
48. Taunk P, Das R, Bisen D, Tamrakar RK (2015) Structural characterization and photoluminescence properties of zinc oxide nano particles synthesized by chemical route method. *J Radiat Res Appl Sci* 8(3):433-438.
49. Tettey C, Shin H (2019) Evaluation of the antioxidant and cytotoxic activities of zinc oxide nanoparticles synthesized using Scutellaria baicalensis root. *Sci Afr* 6:e00157.
50. Thomas B, Raj MC, Joy J, Moores A, Drisko GL, Sanchez C (2018) Nanocellulose, a versatile green platform: from biosources to materials and their applications. *Chem Rev* 118(24):11575-11625.
51. Tomczak MM, Gupta MK, Drummy LF, Rozenzhak SM, Naik RR (2009) Morphological control and assembly of zinc oxide using a biotemplate. *Acta Biomater* 5(3):876-882.
52. Ul-Islam M, Khattak WA, Ullah MW, Khan S, Park JK (2014) Synthesis of regenerated bacterial cellulose-zinc oxide nanocomposite films for biomedical applications. *Cellulose* 21(1):433-447.
53. Wang H, Du H, Liu K, Liu H, Xu T, Zhang S, Chen X, Zhang R, Li H, Xie H (2021) Sustainable preparation of bifunctional cellulose nanocrystals via mixed H2SO4/formic acid hydrolysis. *ACS Chem Biol* 266:118107.
54. Wang TY, Libardo MDJ, Angeles-Boza AM, Pellois JP (2017) Membrane oxidation in cell delivery and cell killing applications. *ACS Chem Biol* 12(5):1170-1182.
55. Wei A, Xiong L, Sun L, Liu Y, Li W, Lai W, Liu X, Wang L, Huang W, Dong X (2013) One-step electrochemical synthesis of a graphene–ZnO hybrid for improved photocatalytic activity. *Mater Res Bull* 48(8):2855-2860.
56. Xu W, Grénman H, Liu J, Kronlund D, Li B, Backman P, Peltonen J, Willför S, Sundberg A, Xu C (2017) Mild Oxalic-Acid-Catalyzed Hydrolysis as a Novel Approach to Prepare Cellulose Nanocrystals. *ChemNanoMat* 3(2):109-119.
57. Yang R-T, Yu HY, Song M-L, Zhou Y-W, Yao JM (2016) Flower-like zinc oxide nanorod clusters grown on spherical cellulose nanocrystals via simple chemical precipitation method. *Cellulose* 23(3):1871-1884.
58. Yu HY, Chen GY, Wang YB, Yao JM (2015) A facile one-pot route for preparing cellulose nanocrystal/zinc oxide nanohybrids with high antibacterial and photocatalytic activity. *Cellulose* 22(1):261-273.
59. Yu HY, Zhang DZ, Lu FF, Yao J (2016) New approach for single-step extraction of carboxylated cellulose nanocrystals for their use as adsorbents and flocculants. *ACS Sustain Chem Eng* 4(5):2632-2643.
60. Yu J, Li C, Liu S (2008) Effect of PSS on morphology and optical properties of ZnO. *J Colloid Interface Sci* 326(2):433-438.
61. Yu M, Yang R, Huang L, Cao X, Yang F, Liu D (2012) Preparation and characterization of bamboo nanocrystalline cellulose. *BioResources* 7(2):1802-1812.

62. Zak AK, Abrishami ME, Majid WA, Yousefi R, Hosseini S (2011) Effects of annealing temperature on some structural and optical properties of ZnO nanoparticles prepared by a modified sol–gel combustion method. *Ceram Int* 37(1):393-398.
63. Zhai J, Sun L, Yu H, Li H, Zhang X, Yang H, Xu J (2014) A facile approach of fabricating graphene-encapsulated ZnO microspheres and their synergic effect on photocatalytic performance. *J. Nanoparticle Res* 16(6):1-10.
64. Zhang G, Liu Y, Morikawa H, Chen Y (2013) Application of ZnO nanoparticles to enhance the antimicrobial activity and ultraviolet protective property of bamboo pulp fabric. *Cellulose* 20(4):1877-1884.
65. Zhao D, Zhu Y, Cheng W, Chen W, Wu Y, Yu H (2021) Cellulose-based flexible functional materials for emerging intelligent electronics. *Adv Mater* 33(28):2000619.
66. Zheng T, Pilla S: Melt processing of cellulose nanocrystal-filled composites (2020) Toward reinforcement and foam nucleation. *Ind Eng Chem Res* 59(18):8511-8531.

Scheme 1

Scheme 1 is available in the Supplementary Files section.

Figures

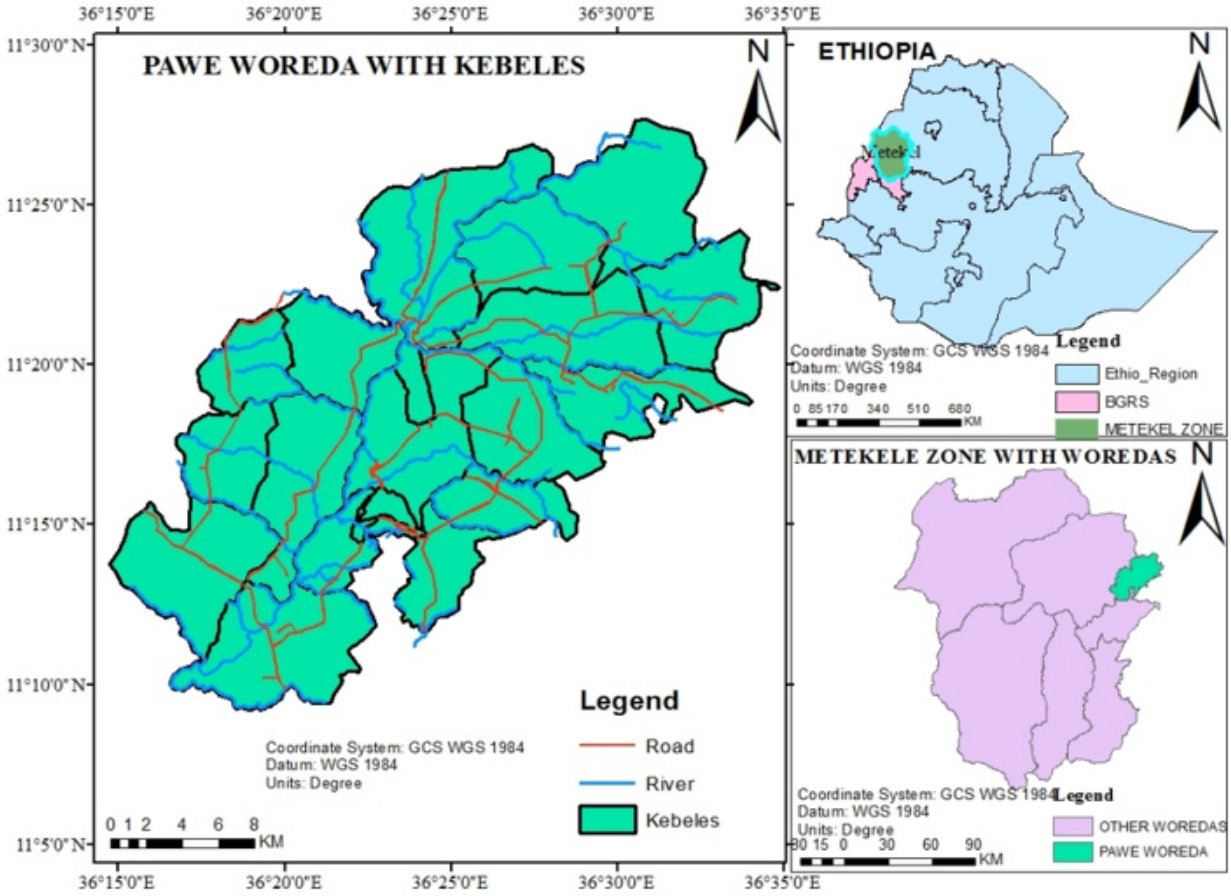


Figure 1

Map of the study area (pawe woreda, Metekel zone, western part of Ethiopia)

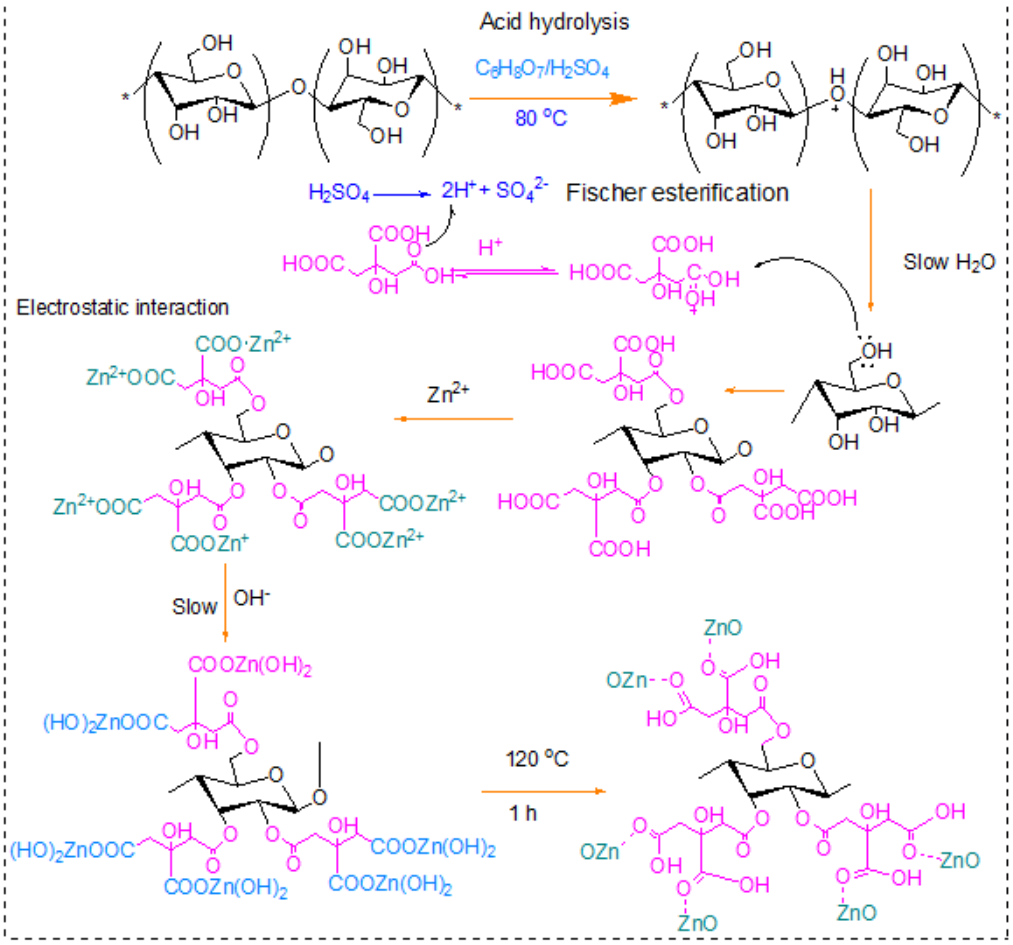


Figure 2

Reaction mechanism for the synthesis of CNC/ZnO nanohybrids

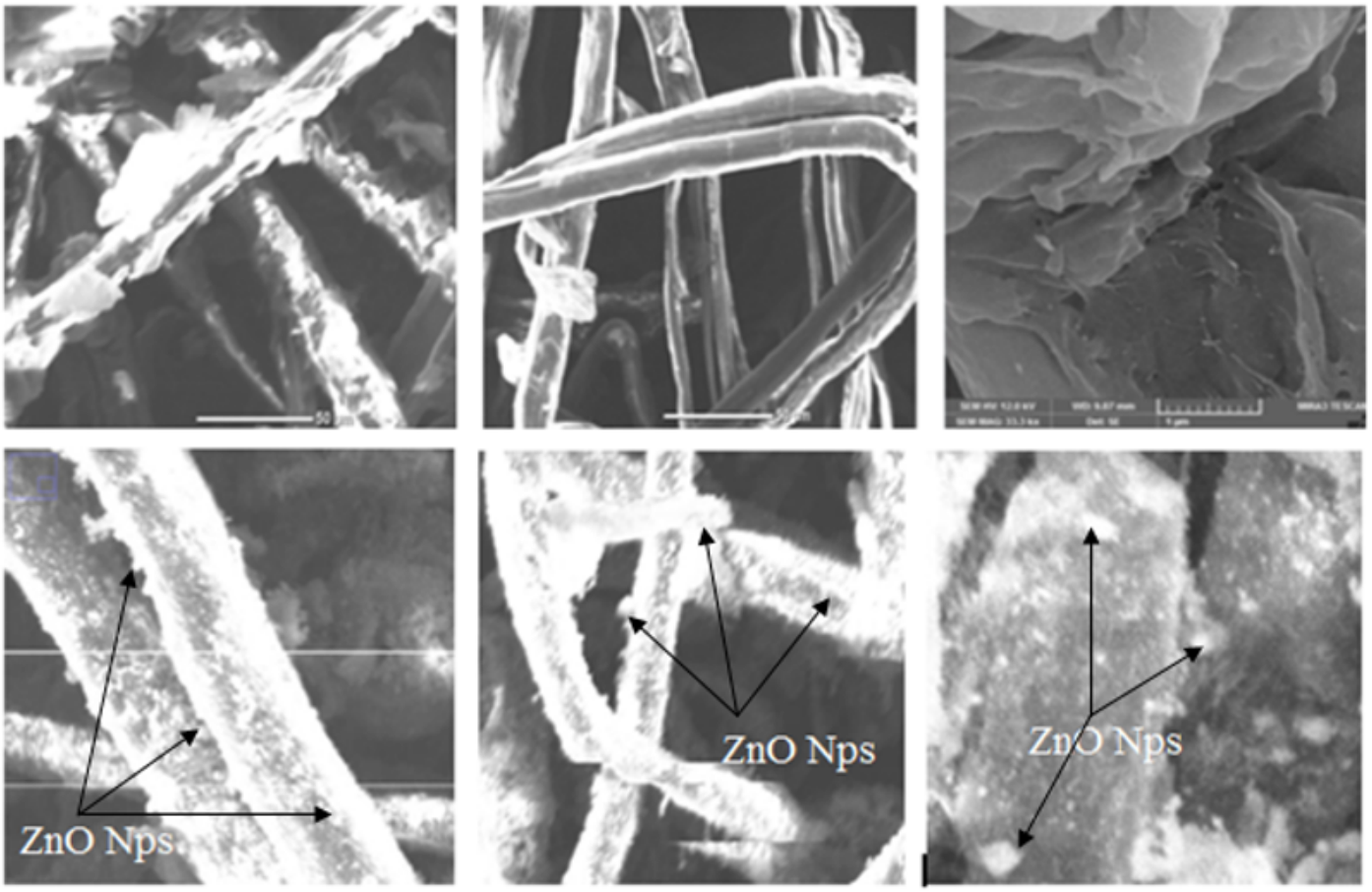


Figure 3

SEM image of ROA (a), COA (b), CNC (c), CNC/$ZnO_{1/2}$ (d), CNC/$ZnO_{3/4}$ (e) and CNC/ZnO_1 (f).

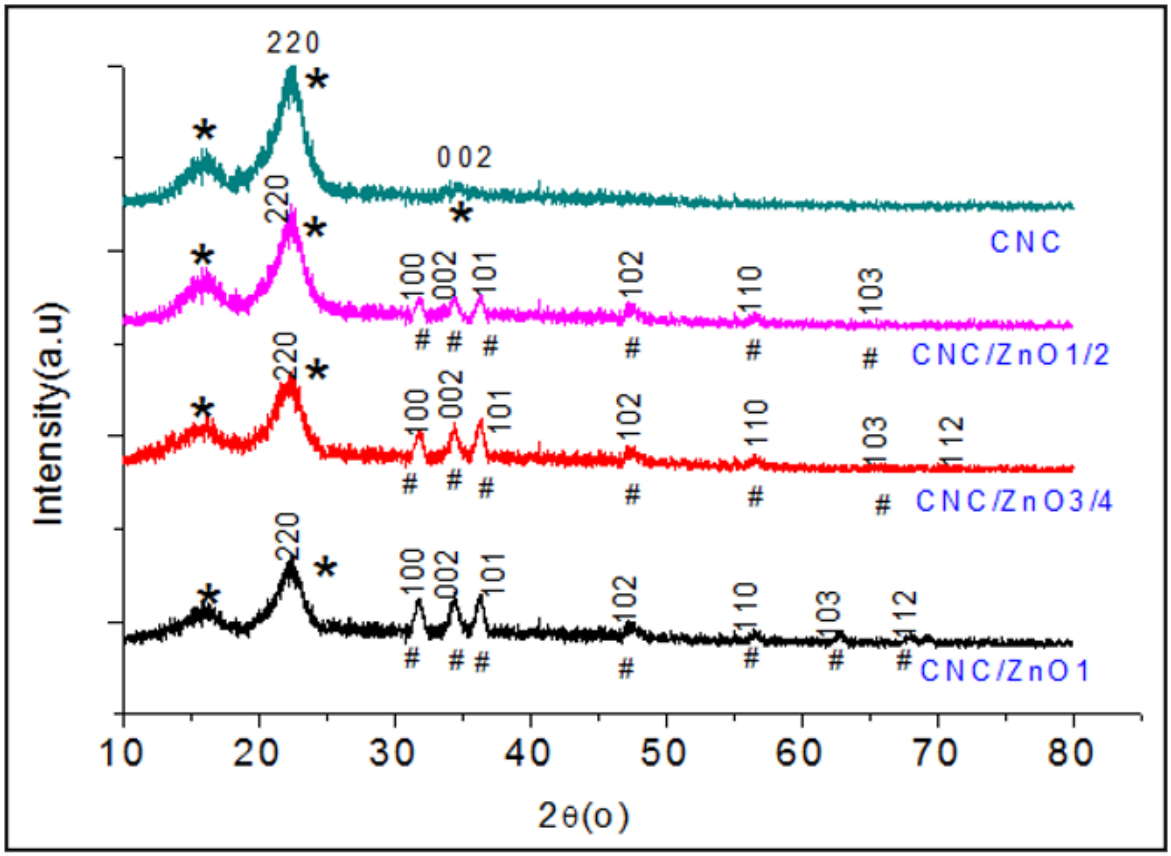


Figure 4

XRD image of CNC and CNC/ZnO samples

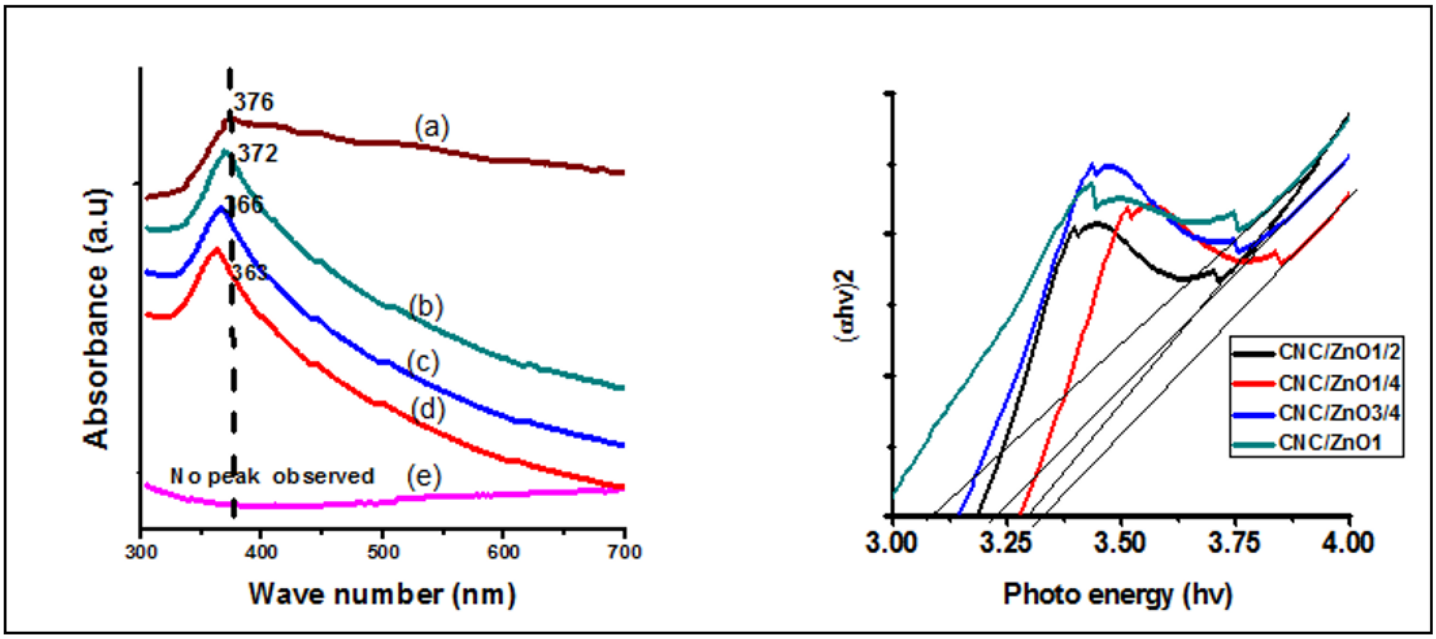


Figure 5

Peak of UV–Vis (left) and its band gap (right) of CNC and CNC/ZnO nanohybrids. Where (e): CNC; (d): CNC/$ZnO_{1/4}$; (c); CNC/$ZnO_{1/2}$; (d); CNC/$ZnO_{3/4}$; (a); CNC/ZnO_1

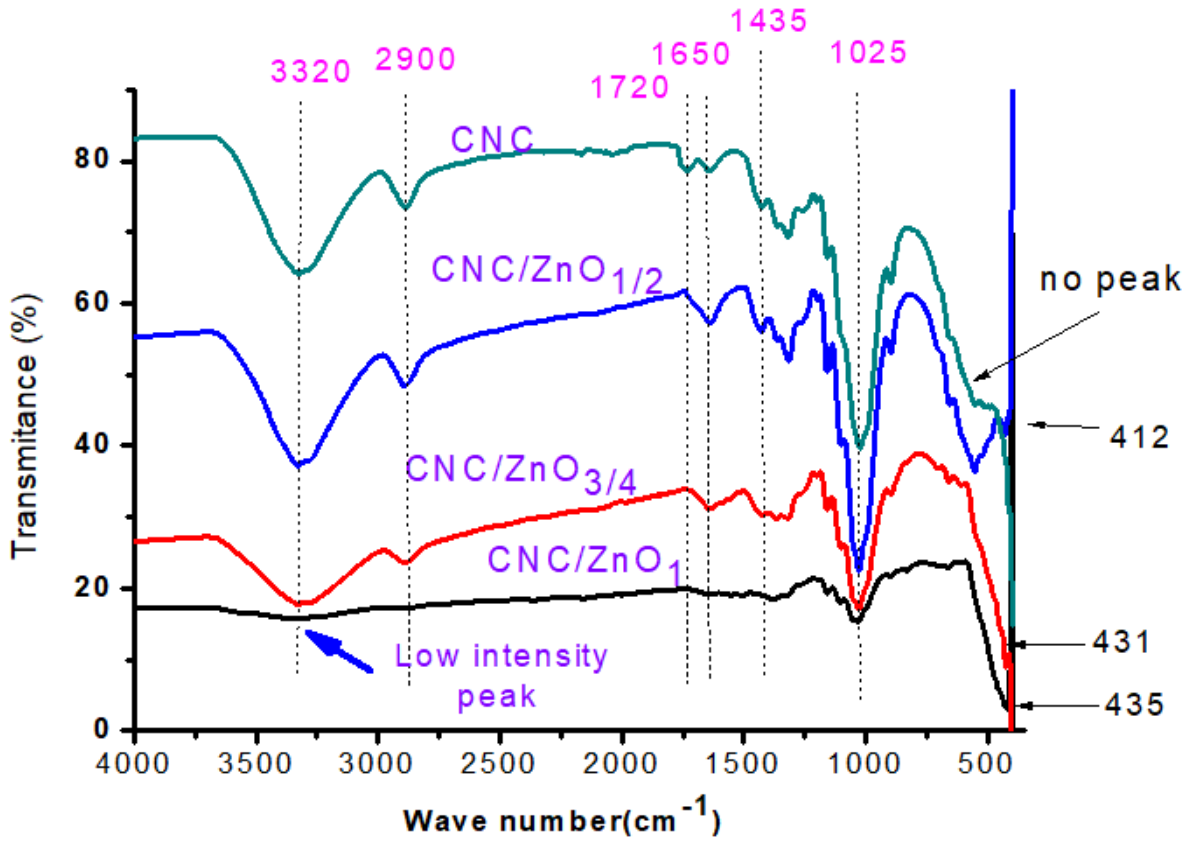


Figure 6

CNC/ZnO and CNC FTIR spectra samples

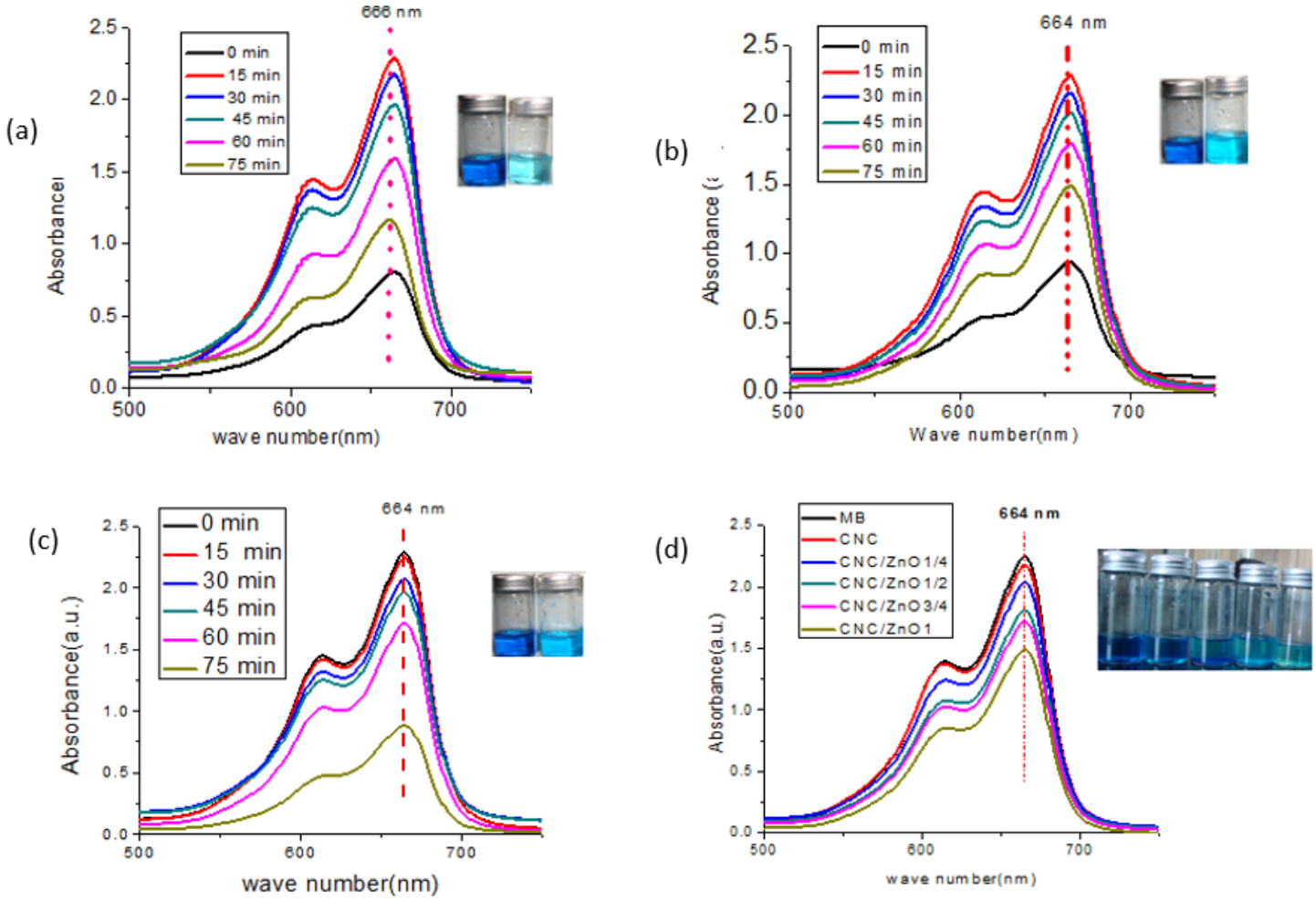


Figure 7

UV-Vis spectrum alterations in the MB using the CNC/ZnO nanohybrid at varied UV-Vis light exposure durations (0, 15, 30, 45, 60, and 75 min). (a) CNC/ZnO_1, (b) CNC/$Zno_{3/4}$, (c) CNC/ZnO½ and (d) six different samples

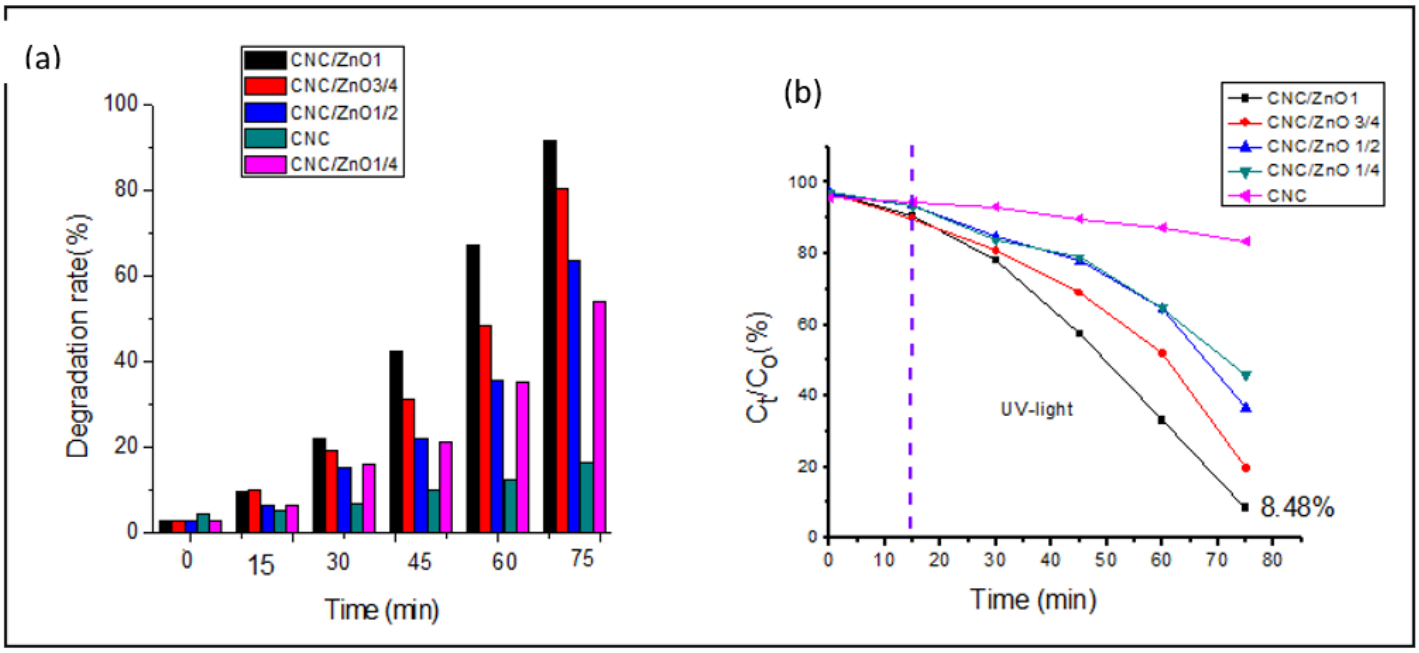


Figure 8

Degradation rate (a) and degradation percentage (b) of ZnO/CNC nanohybrids.

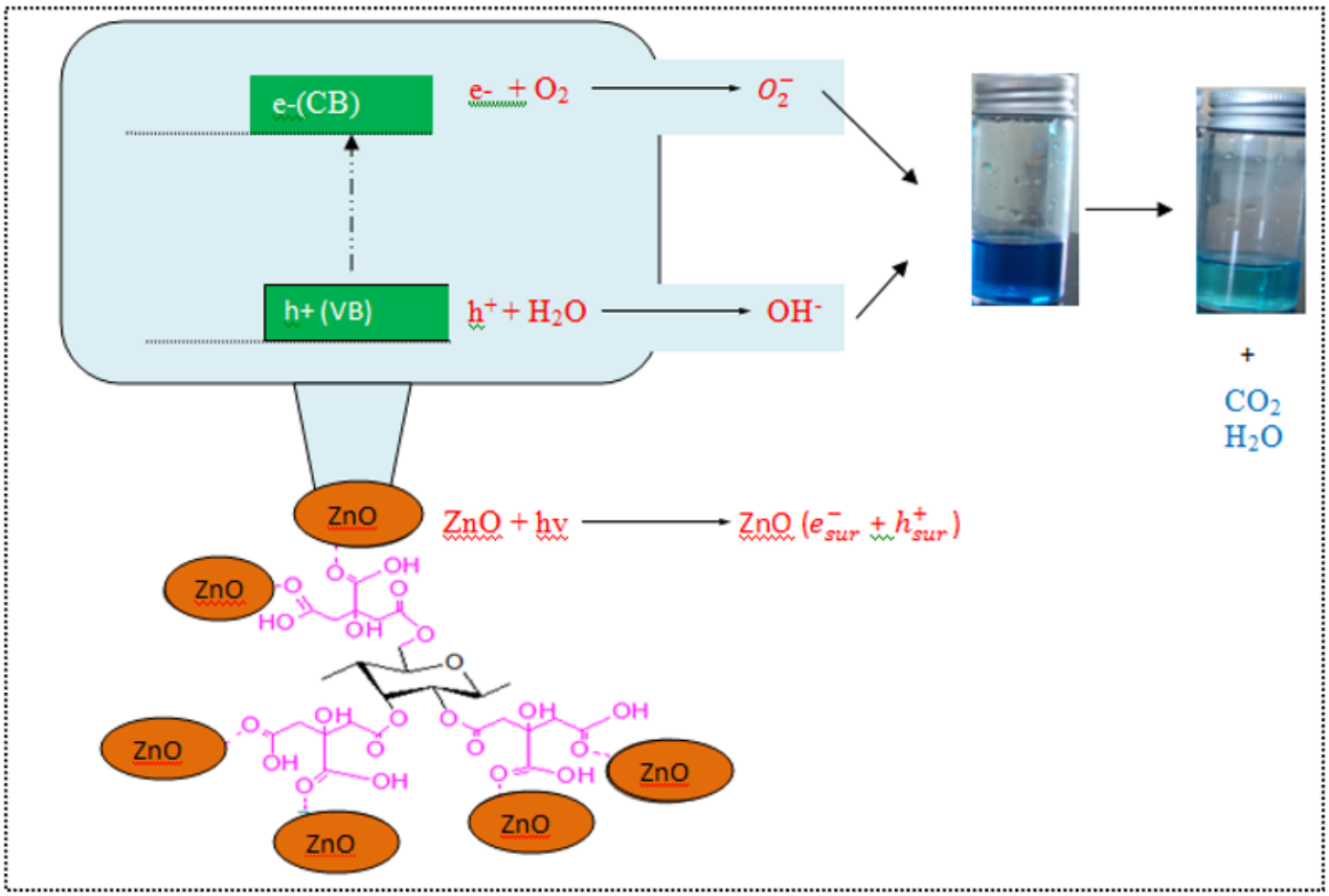


Figure 9

CNC/ ZnO nanohybrids mechanism of photocatalytic activity

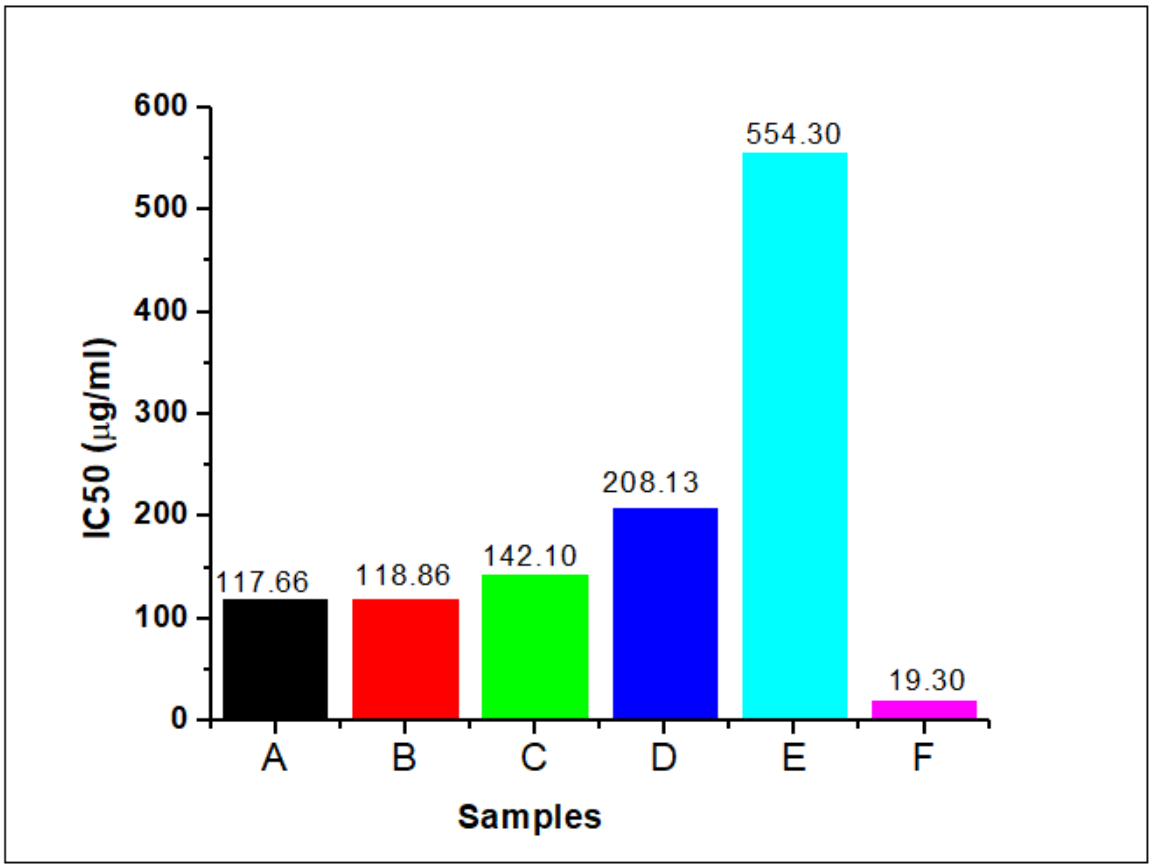


Figure 10

IC50 value of CNC/ZnO_1 (A), CNC/$ZnO_{3/4}$ (B), CNC/$ZnO_{1/2}$ (C), CNC/$ZnO_{1/4}$ (D), CNC (E) and AA (F). *All data were examined in triplicate, and the mean value* ± SD.

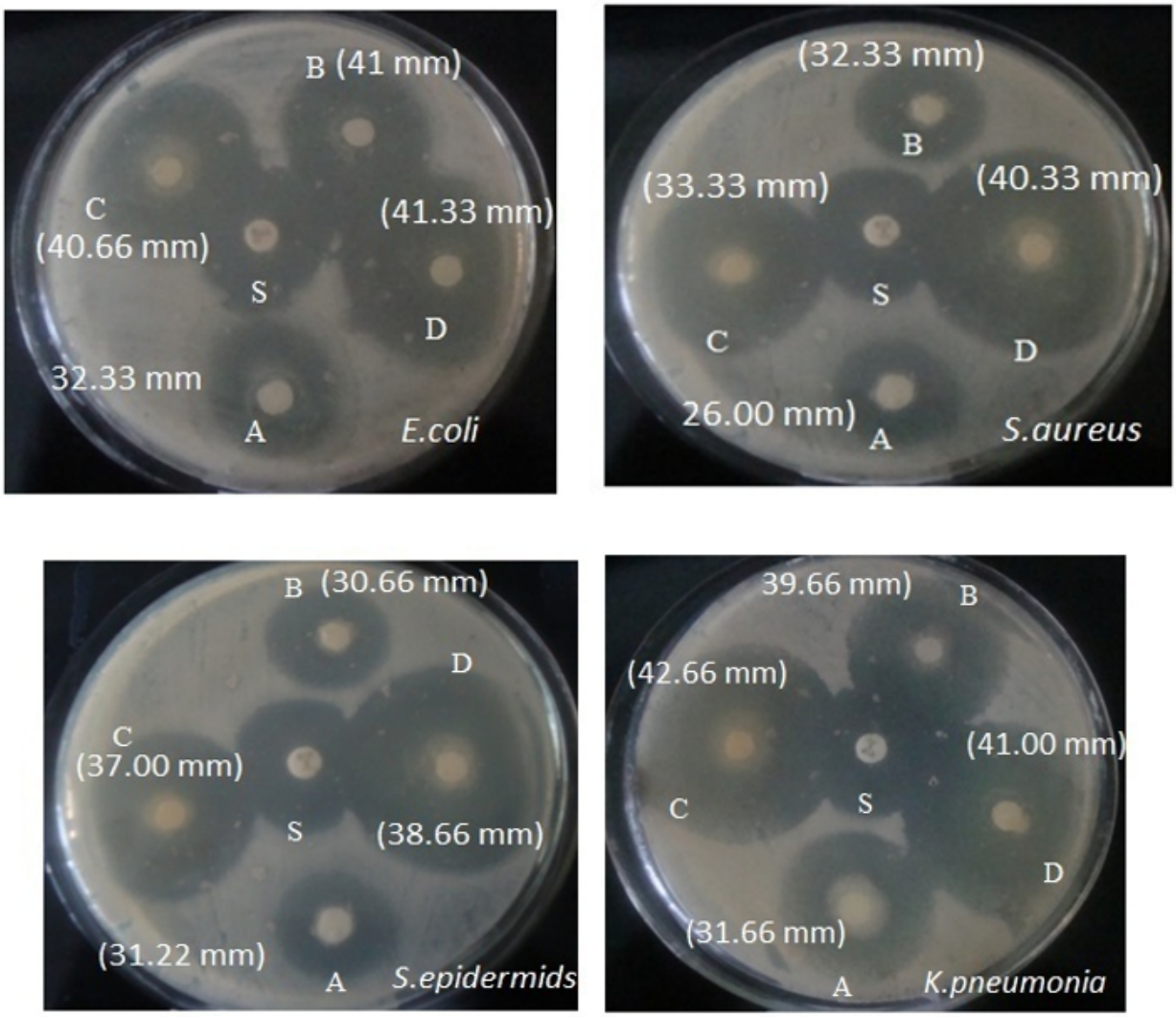


Figure 11

The zone of inhibition exhibited by CNC/ZnO against four bacteria species *Klebsiella pneumonia, Staphylococcus epidermidis Escherichia coli, and Staphylococcus aureus. (A)CNC/$ZnO_{1/4}$, (B) CNC/$ZnO_{1/2}$, (C) CNC/$ZnO_{3/4}$, and (D) CNC/ZnO_1.*

Supplementary Files

This is a list of supplementary files associated with this preprint. Click to download.

- GA.png
- Scheme1.png